A comprehensive analysis of flagellar mutations in *Vibrio cholerae*: Trade-off mechanisms between motility loss and host adaptability

Guozhong Chen [a,b,1], Zixin Qin [a,1], Fenxia Fan [c,1], Mei Luo [a,1], Hongou Wang [d], Baoshuai Xue [e], Shucheng Li [b], Shiyong Chen [f], Xiaoman Yang [a], Xiang Mao [g], Liwen Yi [a], Chunrong Yi [a], Wei Li [a, *], Xiaoyun Liu [d,h,**], Biao Kan [c, ***], Zhi Liu [a, *]

[a]Key Laboratory of Molecular Biophysics of the Ministry of Education/Department of Biotechnology, College of Life Science and Technology, Huazhong University of Science and Technology, Wuhan, Hubei 430074, China.
[b]State Key Laboratory of Microbial Technology, Shandong University, Qingdao, Shandong 266237, China.
[c]National Key Laboratory of Intelligent Tracking and Forecasting for Infectious Diseases, National Institute for Communicable Disease Control and Prevention, Chinese Center for Disease Control and Prevention, Beijing 102206, China.
[d]Department of Microbiology and Infectious Disease Center, NHC Key Laboratory of Medical Immunology, School of Basic Medical Sciences, Peking University Health Science Center, Beijing 100191, China.
[e]Key Laboratory of Zoonosis, Ministry of Education, College of Veterinary Medicine, Jilin University, Changchun, Jilin 130015, China.
[f] School of Marine Science and Engineering, Qingdao Agricultural University, Qingdao, Shandong 266109, China.
[g]Institute of Hygiene Toxicology, Wuhan Centre for Disease Prevention and Control, Wuhan, Hubei 430024, China.
[h]Department of Infectious Diseases, Peking University Third Hospital, Beijing 100191, China.

*Corresponding author: Key Laboratory of Molecular Biophysics of the Ministry of Education/Department of Biotechnology, College of Life Science and Technology, Huazhong University of Science and Technology, Wuhan, Hubei 430074, China.

**Department of Microbiology and Infectious Disease Center, NHC Key Laboratory of Medical Immunology, School of Basic Medical Sciences, Peking University Health Science Center, Beijing 100191, China.

Department of Infectious Diseases, Peking University Third Hospital, Beijing 100191, China.

***National Key Laboratory of Intelligent Tracking and Forecasting for Infectious Diseases, National Institute for Communicable Disease Control and Prevention, Chinese Center for Disease Control and Prevention, Beijing 102206, China.

E-mail addresses: hulwei_009@163.com (W. Li), xiaoyun.liu@bjmu.edu.cn (X. Liu), kanbiao@icdc.cn (B. Kan), zhiliu@hust.edu.cn (Z. Liu)
[1] These four authors contributed equally to this work.

Abstract

Cholera, caused by *Vibrio cholerae*, is characterized by severe watery diarrhea and poses a significant threat to global public health and the aquaculture industry. The flagellum of *V. cholerae* serves not only as a motility organelle for host seeking and colonization but also as a key environmental sensor and signal transducer, directly regulating virulence and biofilm formation. Despite its central role, the trade-off mechanisms between motility loss and enhanced host adaptability remain poorly understood. To address this, we analyzed 3,135 cholera-related samples and found that flagellar mutations in *V. cholerae* cluster primarily in genes such as *flhB*, *fliA*, *fliF*, *fliD*, and *fliM*. Using a flagellar mutant library, we observed that colonization ability was inversely correlated with FlgM secretion. Mechanistically, high intracellular FlgM inactivates the σ^{28} factor FliA, leading to transcriptional derepression of the quorum-sensing master regulator *hapR*. HapR in turn upregulates methionine metabolism and transport, thereby enhancing *V. cholerae* colonization in vivo. Through further validation with a uniquely constructed 6N-labeled mutant pool in an adult mouse model, we demonstrated that motility loss promotes environmental adaptability via the FlgM-FliA-HapR-methionine axis. Our study demonstrates that the secretion level of the flagellar regulator FlgM drives an adaptive shift in *V. cholerae* from motility to colonization within the host. This shift is mediated through quorum sensing and methionine metabolic reprogramming, revealing a novel mechanism that provides new insights into bacterial evolution and pathogenicity.

Keywords: *Vibrio cholerae*, flagellum, FlgM, quorum sensing, methionine metabolism

1. Introduction

Cholera, caused by *Vibrio cholerae*, is characterized by severe watery diarrhea that can be lethal. Infection occurs through the consumption of contaminated food or water. Since 1817, there have been seven global pandemics that resulted in massive human deaths, substantial economic losses and considerable healthcare burdens [1]. The WHO reports a large number of cholera cases or outbreaks, from 44 countries in 2022 to 45 countries in 2023, which poses a serious challenge of cholera prevention and control [2].

The life cycle of *V. cholerae* is closely linked to its pathogenic mechanism. Initially, the bacteria enter the host via contaminated water, survive gastric acid, and colonize the small intestine. Subsequently, their flagella facilitate penetration of the mucus layer, allowing access to the intestinal epithelial surface. As infection progresses, *V. cholerae* forms biofilms and employs quorum-sensing regulation. Upon reaching high cell density, the bacteria detach from the epithelial surface, enter the intestinal lumen, and are ultimately excreted in host feces. They then return to aquatic environments, thereby completing the transmission cycle [3, 4].

V. cholerae is a Gram-negative bacterium with a single polar flagellum, by which it swims rapidly and this motility contributes to quick transmission among different habitats [5,6]. As the propeller of *V. cholerae* movement, the flagellum is a sophisticated device composed of many different structural and functional components. Its biosynthesis involves expression of proteins involved in a series of fine and accurate regulations, acting on transcriptional, translational, and post-translational levels [7]. Transcriptional regulation of *V. cholerae* genes has been well-studied, and is built upon a four-tiered transcriptional hierarchy [3]. The flagellum of *V. cholerae* is also involved in many other biological activities, such as promoting adherence [8], influencing the infectivity [9], triggering c-di-GMP production [10], and sensing mucus layer mechanical attraction [4]. Interestingly, a high number of single nucleotide polymorphisms (SNPs) were detected in the Haiti and Nepal isolates of the 7th cholera pandemic, with 7 out of 54 high quality SNPs belonging to flagellum-associated genes [11]. Similarly, a large number of mutants with impaired motility have been isolated from the laboratory [12-17], the natural environment [18-20], and clinical samples [21]. However, the relationship between motility loss and host adaptability in *V. cholerae* remains unclear.

Here, we analyzed 3,135 cholera-related samples and identified a recurrent pattern of flagellar mutations in *V. cholerae*, with notable clustering in genes including *flhB*, *fliA*, *fliF*, *fliD*, and *fliM*. Screening a flagellar mutant library revealed an inverse correlation between bacterial colonization capacity and FlgM secretion. Mechanistically, elevated intracellular FlgM inhibits the σ^{28} factor FliA, which derepresses transcription of the quorum-sensing master regulator *hapR*. Subsequent upregulation of methionine metabolism and transport by HapR enhances *V. cholerae* colonization in vivo. Using a uniquely constructed 6N-labeled mutant pool in an adult mouse model, we further confirmed that loss of motility promotes host adaptability through the FlgM-FliA-HapR-methionine regulatory axis. Together, our data will shed light on trade-off mechanisms between motility loss and host adaptability.

2. Materials and methods

2.1 In silico analysis flagellar gene mutations in V. cholerae

A total of 3,135 samples in Table S1 were retrieved from the NCBI SRA database by searching for "cholera" or "Vibrio cholerae" in combination with metagenomics-related keywords. These valid sequencing runs were selected for subsequent analysis of flagellar gene mutations. For each dataset, raw reads were quality-filtered using fastp v0.23.2 [22] and assembled with metaWRAP v1.3.2 [23]. Resulting contigs were binned and taxonomically classified using GTDB-Tk v2.4.0 [24]. Bins identified as *V. cholerae* were retained for protein prediction with Prodigal v1.2.6 [25]. A custom reference library of 51 flagellar proteins in Table S2 was constructed based on the *V. cholerae* N16961 genome. Flagellar mutations across 1258 assembled *V. cholerae* bins were then identified in Table S3 and quantified using DIAMOND BLASTP v0.9.30-3 [26]. As controls, the *hapR* gene (which carries a frameshift mutation in N16961)

118 served as a positive control, while the housekeeping
119 genes *asd* (VC2107), *mdh* (VC0432), and *dnaE* (VC2245) were used as negative
120 controls, respectively [27,28].

121 *2.2 Bacterial strains, plasmids, and growth conditions*

122 All *V. cholerae* mutants were derived from strain E1 Tor C6706 and cultured in Luria-
123 Bertani (LB) medium, M9 minimal medium containing 2 mM $MgSO_4$, 0.1 mM $CaCl_2$
124 and 0.2% casein acid hydrolysate, or defined medium containing appropriate antibiotics
125 (streptomycin 100 μg mL^{-1}, kanamycin 50 μg mL^{-1}, ampicillin 100 μg mL^{-1},
126 chloramphenicol 25 μg mL^{-1} for *E. coli* and 1.0 μg mL^{-1} for *V. cholerae*) at 37 °C unless
127 otherwise noted. This defined medium was prepared with the omission of Met and
128 supplementation with 0.5% glucose [29]. In-frame deletion mutants were constructed
129 by cloning the regions flanking a target gene into suicide vector pWM91 that contains
130 a *sacB* counter-selectable marker [30]. Complementation of *flgM* was achieved by
131 inserting P_{lac}-*flgM* into chromosomal *lacZ* using the suicide plasmid pJL1 [31].
132 Overexpression of *flgM* was obtained by cloning *flgM-his*$_6$ downstream of the *tac*
133 promoter of pMal-c2x. Plasmid pBAD24 containing a pBAD-inducible promoter was
134 used to overexpress *flgM-his*$_6$, *flhB*, *flaA-his*$_6$, *fliA-flag*, and *hapR-flag*. The fragment
135 of pBAD-*fliA-flag* was cloned into pYM24 derived from pACYC117 [32], achieving
136 coexistence with the plasmids pMal-*flgM-his*$_6$ and pBBR-*hapR-luxCDABE*. All
137 constructed mutants and plasmids were confirmed by sequencing. All bacterial strains,
138 primers and plasmids used in this study are listed in Table S4&5.

139 *2.3 Motility assay*

140 *V. cholerae* strains were incubated overnight at 37 °C for 12 h. Single colonies were
141 inoculated with sterile toothpicks into LB plates containing 0.3% agar, and these soft
142 agar plates were incubated at 37 °C for 8 h. Photographs were taken and analyzed for
143 colony width as a measure of motility using a gel imaging instrument (GenoSens 1860).

144 *2.4 H_2O_2 killing experiments in vitro*

145 Overnight cultures of flagellar mutants were 1:1,000 sub-cultured into M9 minimal
146 medium containing 2 mM $MgSO_4$, 0.1 mM $CaCl_2$ and 0.2% casein acid hydrolysate
147 and grown at 37°C, 200 rpm until mid-log phase. H_2O_2 was directly added into the
148 cultures at appropriate concentrations, followed by stationary incubation at 37°C for 30
149 min. Serial dilutions of the samples were plated on LB agar for enumeration of colony-
150 forming units (CFU) and the survival rate in presence of H_2O_2 was calculated by
151 comparing CFUs of H_2O_2-challenged and unchallenged samples [32].

152 *2.5 Biofilm formation*

153 Colonies grown on LB agar plates were resuspended in LB broth and grown to an
154 optical density at 600 nm (OD_{600}) of ~0.6. A 1:100 dilution was inoculated into 10 ×
155 75 mm borosilicate glass tubes containing 1 mL M9 minimal medium with 2 mM
156 $MgSO_4$, 0.1 mM $CaCl_2$ and 0.2% casein acid hydrolysate. Biofilms were allowed to
157 form by static incubation at 37 °C for 96 h. The biofilms were stained with crystal violet
158 and quantified with a microplate reader (Spark, Tecan) at 570 nm.

159 *2.6 In vivo colonization assays*

160 All animal experiments were carried out in strict accordance with the animal protocols
161 that were approved by the Ethical Committee of Huazhong University of Science and
162 Technology (Permit Number: SYXK (E) 2022-0094).
163 The streptomycin-treated adult mouse model was used to assess the competition ability
164 of mutants or complement strains during co-colonization with C6706 WT. ROS
165 resistance in the adult mice assay was performed as previously described [33]. For this,
166 five-week-old CD-1 mice were provided with drinking water with or without 10 g L^{-1}
167 of the antioxidant N-acetylcysteine for one week. Afterwards, 5 g L^{-1} streptomycin and
168 0.05 g L^{-1} aspartame were added to the drinking water. One day after streptomycin
169 treatment, the mice were administrated with 100 μL of 10% (w/v) $NaHCO_3$ followed
170 by 100 μL of a 1:1 mixture of WT and mutant (approximately 10^9 CFU for each strain
171 per mouse). Fecal pellets were collected from each mouse at 1, 3, and 5 days after
172 gavage, homogenized, serially diluted in LB and plated on LB agar containing
173 streptomycin and 5-bromo-4-chloro-3-indolyl-β-D-galactopyranoside (X-Gal) to
174 quantify the bacterial loads. The competition index CI was calculated as the ratio of
175 mutant to WT colonies normalized with the input ratio.
176 Five-day-old CD-1 mice were transferred to an incubator and left to adapt for 2 h at
177 30 °C before inoculation. The mice were then administrated with a 50 μL of a 1:1
178 mixture of WT and mutant *V. cholerae* (approximately 10^6 CFU for each strain per
179 mouse) and returned to the 30 °C incubator. The animals were sacrificed 18 h after
180 gavage. Samples of the small intestine were removed and homogenized in 1.5 ml of LB,
181 serially diluted, and plated on LB agar containing streptomycin and X-Gal for
182 quantification of bacterial load. The CI was calculated as the ratio of mutant to WT
183 colonies normalized with the input ratio.

184 *2.7 Growth curve determination and luminescence detection*

185 Overnight LB cultures of targeted strains (with or without plasmid) were inoculated in
186 fresh medium at a ratio of 1:100 and grown with shaking to mid-log phase at 37 °C.
187 The bacteria were harvested by centrifugation, washed three times and resuspended to
188 an OD_{600} of 1.0 with fresh pre-warmed medium (LB or M9), and then diluted 1:1,000
189 in 96-well microplates that were incubated at 37 °C under shaking. The growth kinetics
190 were determined by measuring OD_{600} or OD_{655} using a microplate reader (Spark, Tecan)
191 combined (where applicable) with luminescence detection. If necessary, 0.1 mM

192 isopropyl-β-D-thiogalactoside (IPTG) or 0.2% arabinose was added. Readouts were
193 performed every 30 min for 20 h. The luminescence assay was standardized at OD_{600}.
194 All experiments were performed in triplicate.

195 *2.8 Transmission electron microscopy (TEM) imaging*

196 Single colonies of target strains were inoculated into 50 μL of saline and gently mixed
197 with a clipped, sterile pipette tip. Five microliters of sample were added to a copper
198 supporting mesh. Excess liquid was removed after standing in a ventilated and clean
199 environment for 5 min. The mesh was stained with freshly prepared 1%
200 phosphotungstic acid for 2 min. Excessive dye was removed and the mesh was dried
201 for approximately 1 h prior to transmission electron microscopy (HT7700, HITACHI).

202 *2.9 Secretion of FlgM*

203 To investigate the secretion of FlgM, culture supernatant of the *V. cholerae* mutants
204 containing pBAD24-*flgM-his*$_6$ was collected and the protein was detected according to
205 a previous method with slight modification [4]. All mutant sediment samples were
206 standardized with CFU (10^9). Proteins in the 400mL supernatant were concentrated
207 with 20% trichloroacetic acid (TCA). These, together with the proteins in the precipitate
208 and supernatant were separated by SDS-PAGE, transferred to a polyvinylidene fluoride
209 (PVDF) membrane. The proteins on the Western blot were detected with primary 6×
210 His-tagged rabbit antibodies at a dilution of 1:5,000, and as secondary antibody
211 horseradish peroxidase [HRP]-conjugated goat anti-rabbit immunoglobulin G was used
212 at a dilution of 1:10,000. Immunoblotting was performed using the Pierce ECL Western
213 Blotting Substrate Kit (Thermo Scientific).

214 *2.10 Proteomic analysis*

215 Overnight LB cultures were inoculated 1:100 in fresh LB medium and incubated until
216 OD_{600} reached 0.9 (approximately 10^9 CFU per sample). Then the culture was
217 centrifuged. The pellets were for bacterial proteome samples. For the analysis of the
218 bacterial secretome, the 400 mL of culture supernatant was filtered through a 0.22 μm
219 microporous membrane to remove intact bacteria. The proteins in the filtrate were
220 precipitated overnight at 4 °C with 20% TCA containing 0.5 mM sodium deoxycholate.
221 After centrifugation at 10,000 g for 1 h at 4 °C, the protein pellets were washed three
222 times with cold acetone for LC-MS/MS experiments, that were carried out as previously
223 described [32]. The secretome experiments were performed in duplicates, and bacterial
224 proteome samples were analyzed in triplicates. Proteins with Fold changes >1.5 and $P<$
225 0.05 were considered as significant differences.

226 *2.11 Gene expression analysis via RT-PCR and qPCR*

227 Overnight LB cultures were inoculated 1:100 in fresh LB medium containing
228 appropriate antibiotics or, if needed, 0.2% arabinose, and incubated at 37 °C. RNA for

229 real-time PCR (RT-PCR) was extracted using an RNA extraction kit. The RT-PCR
230 reaction was performed using SYBR green fluorescent dye and CFX Connect Real-
231 time Detection System (Bio-Rad). The genes *recA* or *secA* or 16S rRNA were used for
232 normalization. Relative expression levels were calculated using the $2^{-\Delta\Delta CT}$ method. All
233 experiments were performed in triplicate. For reverse transcription, approximately 400
234 ng of RNA was extracted using the HiScript II 1st Strand cDNA Synthesis Kit. The
235 RT-qPCR primers used for detection of mRNA of specific genes are listed in Table S5.
236 All primers were tested for PCR specificity and efficiency.

237 *2.12 Protein purification*

238 The proteins HapR-His_6 were expressed in *E. coli* BL21 (DE3) and purified using the
239 pET system and BeyoGold™ His-tag Purification Resin (P2218, Beyotime).

240 *2.13 EMSA*

241 The purified recombinant proteins HapR containing 6×His-tags were used for EMSA.
242 The promoters of their target genes were amplified by PCR and purified. These
243 amplicons (50 ng) were incubated with 6× His-tagged protein in 20 μL containing 4μL
244 of 5× binding buffer (50 mM Tris-HCl, 0.25 M KCl, 2.5 mM DTT, 5 mM $MgCl_2$, 0.25
245 mg mL^{-1} BSA, 2.5 mM EDTA, 1% glycerol, pH 8.3) at 25 °C for 30 min. DNA-protein
246 complexes were analyzed by electrophoresis on a 5% native polyacrylamide gel at 4 °C
247 and 80 V cm^{-1} for 1.5 h. After staining the gel in ethidium bromide for 10 min, a gel
248 imaging system (GenoSens 1860) was used to produce images. The EMSA primers
249 used in this study are listed in Table S5.

250 *2.14 Synthesis of fluorescent monomers*

251 FITC-D-Glucose was synthesized as previously described [34]. Briefly, D-glucosamine
252 hydrochloride (77.6 mg, 0.36 mmol, 1.2 equiv) and Et3N (91.1 mg, 0.9 mmol, 3.0 equiv)
253 were mixed in DMF (10 mL). After 1 h of stirring, fluorescein (116.8 mg, 0.3 mmol,
254 1.0 equiv) was added. The reaction mixture was stirred for 16 h at RT in the dark, after
255 which the solid product was obtained by filtering and concentrated *in vacuo*.

256 *2.15 Bacterial metabolic activity assay in vitro*

257 Bacterial cultures in LB were harvested at OD_{600} ~0.4 by centrifugation and the cell
258 pellet was washed 3 times with Met-free MM medium. The cells were resuspended and
259 incubated at 37°C for 30 minutes. A solution of 10 mL Met-free MM medium and 1 μL
260 of FITC-D-Glu was added and 500 μL of this was added to transwell wells and 200 μL
261 of this was added to the transwell chambers. To each well, 100 μL of bacterial
262 suspension was added and the plates were incubated for 30 min at 37 °C in the dark.
263 The supernatant was washed off with PBS buffer and then assayed by Flow Cytometry.

264 *2.16 Bacterial metabolic activity assay in vivo*

265 Bacterial metabolic activity was assayed in vivo as previously described with following
266 modifications [35]. The CD-1 mice were administered with WT and mutants for
267 competition colonization experiments as described above. At 48 h post-inoculation, the
268 mice were administered with 100 μL FITC-D-Glu (0.1 mM) in PBS. Two hours after
269 the gavage, the animals were sacrificed and the small intestine was dissected and rinsed
270 with 2 mL PBS, cut longitudinally and the intestinal content was scraped off using a
271 cell scraper. The intestinal content was suspended into a 1.5 mL PBS buffer with 2 steel
272 beads and shaken to release bacteria. Centrifugation at 3000 rpm for 1 min removed
273 large tissue fragments and impurities, and the supernatant was filtered through 40 μm
274 cell strainers to remove smaller cell debris. The filtrate was centrifuged (8,000 rpm, 5
275 min), the bacterial pellets were washed twice with 1.5 mL PBS and resuspended in PBS
276 for flow cytometry analysis. In the FITC channel, cells with strong signals of
277 approximately 10% were selected for sorting, with 10^5 events obtained for each sample,
278 and the collected samples were diluted and plated on LB agar containing streptomycin
279 and X-Gal for quantification of the bacterial index.

280 *2.17 Detection of amino acid profiles in Δ*flhB* and Δ*flaA* by HPLC and MS*

281 Overnight LB cultures of Δ*flaA* and Δ*flhB* were sub-cultured with an inoculum of 1:100
282 in MM medium and shaken at 37 °C until OD_{600}=0.5. The bacteria were collected by
283 centrifugation (>200mg) and samples of 60 mg were suspended in 50 μL water,
284 vortexed for 60 s, and mixed with 400 μL methanol-acetonitrile solution (1:1, v/v) and
285 50 μL of a mixture of 16 isotopic internal standards (50 μM). The mixture was vortexed
286 for 60 s and twice subjected to low-temperature ultrasound for 30 min. Proteins were
287 precipitated at -20 °C for 1 h and after centrifugation at 14,000 g and 4 °C for 20 min
288 and the supernatant was collected, freeze-dried, and stored at -80 °C prior to high-
289 performance liquid chromatography (HPLC). HPLC was performed using an Agilent
290 1290 Infinity LC ultra-high-performance liquid chromatography system. The mobile
291 phase consisted of 25 mM ammonium formate + 0.08% formic acid (solution A) and
292 0.1% formic acid acetonitrile (solution B). The samples were loaded into an automatic
293 sampler at 4 °C, and the column temperature was set at 40 °C. The flow rate was 250
294 μL min^{-1}, and the injection volume was 1 μL. The gradient elution was as follows: 0-
295 12 min, linear change from 90% B to 70% B; 12-18 min, linear change from 70% B to
296 50% B; 18-25 min, linear change from 50% B to 40% B; 30-30.1 min, linear change
297 from 40% B to 90% B; 30.1-37 min, maintained at 90% B. At regular intervals between
298 experimental samples a quality control (QC) sample was inserted to evaluate the
299 stability and reproducibility of the system.
300 Mass spectrometry (MS) analysis was performed using a 5500 QTRAP mass
301 spectrometer (SCIEX) in positive ion mode. The ESI source conditions for the 5500
302 QTRAP were as follows: source temperature 500 °C, ion Source Gas 1 (Gas 1): 40, Ion
303 Source Gas 2 (Gas 2): 40, Curtain gas (CUR): 30, IonSapary Voltage Floating (ISVF)
304 5,500 V. The analytes were detected using the MRM mode.

305 *2.18 In vivo colonization assay of 6N-labeled mutants*

306 Briefly, using C6706 (*vc1807*:: CmR) as a template, amplify the CmR fragment and
307 insert a 6N site as a marker in the middle of one end primer (6N-R) [36], then clone it
308 into the pWM91 vector. Sequence tags of 6N were inserted into the *lacZ* position of the
309 26 mutants and the WT strain with the 6N-labeled plasmids pWM91-CmR-6N by
310 conjugation experiments. After labeling the bacterial strains, confirmed by sequencing,
311 they were sub-cultured and adjusted to an OD_{600} of 1.0. After harvesting by
312 centrifugation, the bacterial pellets were stored at -20°C. Using the methionine-
313 supplemented and water-restricted mouse model, the mice were gavaged with 100 μL
314 of the mixed bacterial samples per mouse. On day 5 after gavage, mouse feces were
315 collected and total DNA was extracted, along with the input samples. Amplicons
316 produced by PCR with primers targeting both ends of *LacZ* were sequenced. The
317 sequenced raw data was analyzed by Vsearch for merging paired-end reads and Python
318 to calculate the proportion of reads from the 6N-labeled mutants among the total reads.

319 *2.19 Statistical analysis*

320 Results are presented as mean ± standard deviation. When two groups were compared,
321 *t*-tests were performed. One-way analysis of variance (ANOVA) was used for two or
322 more treatment groups. Statistical analysis was performed using the software GraphPad
323 Prism v.9 for Windows. Differences with a p value less than 0.05 were considered to
324 be statistically significant.

325 **3. Results**

326 *3.1 High-frequency mutations in the flagellar genes of V. cholerae*

327 The life cycle of *V. cholerae* primarily alternates between aquatic environments and the
328 human host [3]. To investigate its adaptation across these niches, we categorized
329 cholera-related metagenomic sequencing samples from the SRA database in Table S1
330 into five groups based on their origin: human, clinical, aquatic (including water and
331 sewage), fish, and amoeba-derived. These samples were collected from 19 countries
332 (Fig. 1A). A total of 1,258 metagenome-assembled genomes (MAGs) of *V. cholerae* in
333 Table S3 were reconstructed from these samples. Their flagellar protein mutations were
334 then systematically analyzed using the 51 flagellar proteins of *V. cholerae* N16961 in
335 Table S2 as reference amino acid sequences. For quality control, the mutation-
336 prone *hapR* gene, which carries a frameshift mutation in the N16961 genome, served
337 as a positive control, while the conserved housekeeping
338 genes *asd* (VC2107), *mdh* (VC0432), and *dnaE* (VC2245) were used as negative
339 controls, as established in prior studies [27,28].
340 Our mutation frequency analysis revealed that across all sampled habitats, flagellar
341 gene mutations in *V. cholerae* consistently clustered in key genes,
342 including *flhB*, *fliA*, *fliF*, *fliD*, and *fliM* (Fig. 1B). Notably, mutations were also

343 detected in the primary flagellar regulator gene *flrA*, a finding consistent with previous
344 reports [16,37]. Functionally, these mutated genes are involved in critical flagellar
345 structures and regulatory hierarchies, including Class I and IV transcriptional regulation,
346 the type III secretion system (T3SS) apparatus, the filament-capping complex, and the
347 C-ring switch structure (Figure 1C, D). This indicates that these loci have key
348 evolutionary and pathological significance in regulating the host adaptability balance.

349 *3.2 Phenotypic screening of the flagellar mutant library*

350 To elucidate the environmental adaptability conferred by the flagellar gene mutations
351 identified through the above big data-driven analysis, a systematic mutant library
352 targeting 26 flagellar-related regulons of *V. cholerae* listed in Table S4 was constructed.
353 Subsequently, this library was subjected to comprehensive phenotypic screening,
354 assessing motility, biofilm formation, growth rates in both rich and minimal media,
355 colonization efficiency in infant and adult mice, as well as resistance to H_2O_2. The H_2O_2
356 assay is particularly relevant as it reflects bacterial survival under host-derived reactive
357 oxygen species (ROS) stress. Of the investigated mutants, 22 mutants had completely
358 lost their motility. Deletion of chemotaxis-related genes *cheV-3*, *flgO* and *flgP* resulted
359 in significantly impaired motility (Fig. 2A, Supplementary Fig. S1), which is consistent
360 with previous reports [6, 38]. The colonization ability in infant mice was seriously
361 damaged (Supplementary Fig. S2) and biofilm formation of the 26 mutants were mostly
362 enhanced, which were consistent with earlier findings (Supplementary Fig. S3) [5,6,10].
363 Surprisingly, we observed completely opposite results in the adult mice, as some of the
364 mutants were able to outcompete the WT strain (Fig. 2B), although their growth rates
365 were consistently lower than that of WT in minimum or rich medium (Supplementary
366 Fig. S4 and S5), and others were attenuated. In total, five mutants (Δ*flgBCDE*, Δ*fliK*,
367 Δ*fliKLMNOPQRflhB*, Δ*fliE,* and Δ*flgP*) produced no significance difference in CI (blue
368 in Fig. 1D), nine mutants (Δ*flrA*, Δ*rpoN*, Δ*flrC*, Δ*fliEFG*, Δ*fliHIJ,* Δ*fliA*, Δ*flgFGHIJ,*
369 Δ*fliPQR*, and Δ*flhB*) displayed enhanced CI (red in Fig. 2B), and twelve mutants (Δ*flhA*,
370 Δ*flhA* operon, Δ*flgB*, Δ*motY*, Δ*flaA*, Δ*flgK*, Δ*flgO*, Δ*flgT*, Δ*cheV-2*, Δ*vc1384*, Δ*flgM*,
371 and Δ*cheV-3*) were attenuated for CI (green in Fig. 2B). Of these, the Δ*flgFGHIJ* mutant
372 produced the highest CI with a 1000-fold increased CI compared to WT, while the
373 Δ*flgO* mutant had the lowest CI (1/1000-fold of WT). Of the other mutants, Δ*flhB*,
374 impaired in production of the flagellar type III secretion system (fT3SS) protein FlhB,
375 was enhanced in adaptability, and Δ*flaA*, missing the major flagellin filament protein,
376 was attenuated. We furtherly analyzed the various phenotypes of all 26 mutants in more
377 detail, and found that only the colonization potential in the adult mouse model differed
378 among the mutants. All other phenotypes (e.g. motility, biofilm development,
379 proliferation in LB/M9, H_2O_2 resistance, infant mice colonization) exhibited a unipolar
380 distribution. Correlation analysis indicated that adult mice colonization was not
381 associated with other phenotypes (Supplementary Fig. S6).

382 *3.3 FlgM secretion negatively regulating adaptability*

383 Considering FlaA and FlhB are structural flagellar component without a regulatory
384 function, they were confirmed through transmission electron microscopy that the 2
385 mutants lacked flagella (Supplementary Fig. S7A), and that overexpression of the
386 relevant genes restored their motility capability (Supplementary Fig. S7B). So, we
387 choose Δ*flhB*, Δ*flaA* and WT normalized with CFU (Supplementary Fig. S7C) were to
388 explore the underlying mechanism of these opposite colonization properties by
389 sequenced proteins in the supernatant (Fig. 2C). These proteins from Δ*flhB* and Δ*flaA*
390 were compared to a WT normalized control, in an attempt to seeking differentially
391 expressed proteins. This detected 36 proteins that were differently secreted between the
392 Δ*flhB* and Δ*flaA* mutants (Table S6, Supplementary Fig. S7D), including 15 flagellar
393 assembly proteins, 9 cellular processes related proteins, 2 secreted hemolysin proteins,
394 2 cell membrane associated proteins, 2 reactive oxygen species (ROS)-resistance
395 proteins, and 6 other proteins.
396 Hemolysins HlyA and Tlh are secreted toxin proteins that play a role in the virulence
397 of *V. cholerae* [6, 39]. However, their deletions in Δ*flhB* to give Δ*flhB*Δ*hlyA* and
398 Δ*flhB*Δ*tlh*, Δ*flhB*Δ*katG* and didn't affect their CI in the adult mice model
399 (Supplementary Fig. S8A, B). Colonization in this model can also be enhanced by ROS-
400 resistance, for which KatG and catalase are held responsible [32]. Experiments were
401 performed to investigate this, for which N-acetylcysteine (NAC) was employed to
402 remove ROS from the murine intestine (Supplementary Fig. S8C), but this revealed no
403 difference in the CI of Δ*flhB* or Δ*flaA* compared to that in absence of NAC
404 (Supplementary Fig. S8D, E). As not all mutants but the majority are resistant to ROS,
405 this did not seem to explain the enhanced colonization of particular flagellar mutants
406 (Supplementary Fig. S9).
407 Interestingly, the secretion of FlgM in Δ*flhB* was reduced about 9-fold compared
408 with that of Δ*flaA* (Fig. 2C). FlgM is an anti-σ^{28} factor, and functions as a chaperone
409 protein of σ^{28} factor FliA [40]. Our previous research had demonstrated that FlgM can
410 be secreted by Δ*flgD* through broken flagella, which activates FliA activity, to then
411 repress the expression of *hapR* that subsequently upregulates the expression of
412 virulence gene *tcpA* and enhances *V. cholerae* colonization in infant mice [4].
413 Introduction of a double-mutation where *flgM* was knocked out in a Δ*flhB* background
414 dramatically reversed the Δ*flhB* colonization pattern, from a CI of 176.3293 for Δ*flhB*
415 to 0.0098 for Δ*flhB*Δ*flgM* (P= 0.0005) (Fig. 2D). In addition, the overexpression of
416 FlgM in Δ*flaA* (*lacZ*::P_{lac}-*flgM*) also significantly reversed the phenotype of Δ*flaA*,
417 from CI=0.0130 for Δ*flaA* to 0.2285 for Δ*flaA* (P= 0.0146) (Fig. 2E). Based on these
418 observations, we analyzed FlgM secretion in all 26 mutants and found that this
419 negatively correlated (R^2=-0.4417, P=0.0239) with their CI in adult mice (Fig. 2E, F).
420 Together, these data suggest that changes in intracellular FlgM levels in the various
421 flagellar mutants may contribute to their diverse colonization properties in adult mice.

422 *3.4 Intracellular FlgM drives hapR expression*

423 *V. cholerae* employs cell-to-cell communication, so-called quorum sensing, of which
424 HapR is the master regulator, which is in charge of many important regulation activities
425 in response to different environmental signals [41, 42]. In the Δ*flhB* mutant, a high
426 concentration of intracellular anti-σ^{28} factor FlgM is available to bind to σ^{28} factor FliA,
427 thereby inhibiting its function; this leads to an increase in *hapR* transcription (Fig. 3A,
428 left) [4]. We sequentially knocked out *flgM*, *fliA*, and *hapR* in a Δ*flhB* background.
429 Whereas the double mutant Δ*flhB*Δ*flgM* had a reduced CI (0.0010) compared to Δ*flhB*
430 (CI=210.5072, *P*=0.002), this phenotype was more than reversed in the triple mutant
431 Δ*flhB*Δ*flgM*Δ*fliA* (CI=616.9768), whereas the quadruple mutant
432 Δ*flhB*Δ*flgM*Δ*fliA*Δ*hapR* had a reduced CI (1.408) again (Fig. 3A, right). The order of
433 sequential mutation was then reserved by inactivating (in that order) *flgM*, *fliA*, and
434 *hapR* in a Δ*flaA* background, which resulted in similar switches in colonization ability
435 (Fig. 3B). This suggests that *hapR* expression may be responsible for the different
436 colonization abilities of these flagellar mutants in the applied adult mouse model.
437 This hypothesis was confirmed by determining that the transcription of *hapR* was
438 significantly upregulated in those mutants with enhanced colonization, and
439 significantly downregulated or unchanged in the other flagellar mutants (Fig. 3C). And
440 In addition, the knockout of *hapR* significantly decreased the CI (Fig. 3D), suggesting
441 that a FlgM-FliA-*hapR* pathway contributes to the colonization potential.
442 We found that overexpression of FliA (by means of pBAD-*fliA*) in Δ*flgM*Δ*fliA*
443 significantly repressed *hapR* expression (*P*=0.020), while overexpression of FlgM in
444 Δ*flgM*Δ*fliA* derepressed *hapR* transcription (*P*=0.003) (Fig. 3E). Similar results were
445 obtained with *E. coli* DH5α (Supplementary Fig. S10), suggesting that *hapR* expression
446 may be regulated by FliA directly.
447 Previous studies had reported that the VarS/VarA-CsrA/BCD pathway, three
448 autoinducer systems (CAI-1, AI-2, DPO), and VqmA can regulate *hapR* expression
449 (Fig. 3F) [43-45]. We determined the expression of each key gene within the quorum
450 sensing network in the Δ*fliA* mutant, which suggested that FlgM-FliA may indirectly
451 inhibit HapR degradation through the VarS/VarA-CsrA/BCD pathway (Fig. 3G). To
452 compare the priority of direct and indirect regulation of *hapR* by FlgM-FliA, the *varA*
453 and *hapR* genes were individually knocked out in a Δ*flhB* background. Adult mice
454 colonization results revealed that this drastically reduced colonization compared to
455 Δ*flhB* (*P*=0.0026 for *varA* and *P*=0.0023 for *hapR*); no significantly difference was
456 observed between Δ*flhB*Δ*varA* and Δ*flhB*Δ*hapR* (Fig. 3H). The double mutation of
457 *varA* and *flhB* consistently decreased the expression level of *hapR* (Supplementary Fig.
458 S11). Taken together, it is concluded that interaction between intracellular FlgM and
459 FliA derepresses *hapR* transcription, resulting in an enhanced colonization ability of *V.*
460 *cholerae* in adult mice.

461 *3.5 HapR monitors methionine metabolism*

462 We next compared precipitated protein profiles of Δ*flhB* and Δ*flaA*, using WT as a
463 normalization control in Table S7. The cellular protein levels of flagellin proteins FlaD,

464 methionine sulfoxide reductase MsrC, serine protease VesC, and hypothetical proteins
465 VC1075 were upregulated (Fig. 4A). However, no significantly difference was
466 observed among Δ*flhB* and Δ*flhB*Δ*flaD,* Δ*flhB*Δ*vesC,* Δ*flhB*Δ*vc1075* in the adult mice
467 (Supplementary Fig. S12). The MsrC was the highest enriched cellular protein in Δ*flhB*
468 (Log_2Ratio=3.000, *P*=0.002), relative to Δ*flaA* (Fig. 4A). Therefore, we now
469 hypothesize that cellular methionine contributes to the different colonization patterns
470 of the 26 flagellar mutants in adult mice.
471 In *V. cholerae*, cellular methionine metabolism is finely regulated via biosynthesis,
472 transformation and transportation systems [Fig. 4B] [46]. As expected, the addition of
473 methionine significantly reduced Δ*flhB* and it increased Δ*flaA* colonization in adult
474 mice (Fig. 4C), whereas Δ*msrC* drastically reduced the colonization advantage (Fig.
475 4D, CI=0.015). However, knockout of the methionine biosynthesis genes *msrC* or/and
476 *metR* in a Δ*flhB* background didn't reduce colonization advantage, unless the
477 methionine transportation genes *metI* and *metT* were also inactivated
478 (Δ*flhB*Δ*msrC*Δ*metR*Δ*metI*Δ*metT* *vs.* WT compared to Δ*flhB* *vs.* WT, FC=6.341,
479 *P*=0.001) (Fig. 4E). This suggests that the cellular methionine yield is precisely
480 regulated by a range of metabolic and transportation genes in *V. cholerae*, which is not
481 surprising, since methionine is an essential amino acid for bacterial metabolism and
482 proliferation. Subsequently, the amino acid content in the precipitates of Δ*flaA*, Δ*flhB*,
483 and WT were quantified. We found lower serine concentration (*P*=0.040) and higher
484 concentrations of cystine (a disulfide of two oxidized cysteine molecules, *P*=0.018) in
485 Δ*flhB* compared with Δ*flaA*, but no variation in methionine concentrations could be
486 demonstrated by intracellular amino acid assays (Fig. 4F). Beyond bacterial
487 biosynthesis and uptake, intracellular methionine can also be increased via other amino
488 acid pathways. The KEGG pathway shows that L-cystathionine, a downstream product
489 of serine and methionine, can be converted to cysteine, from which cystine is formed
490 (Fig. 4G) [47], so that a higher active methionine metabolism in Δ*flhB* may relate to
491 lower serine concentrations and higher cystine concentrations. Interestingly, we also
492 found that *hapR* is involved in the expression of enzymes related to other amino acid
493 metabolism by analyzing the transcriptome from our Mr.VC database [48, 49],
494 including serine and cysteine metabolism, suggesting that *hapR* may be involved in the
495 regulation of methionine metabolic flow.
496 Tsou et al. have described that HapR is a global regulator in *V. cholerae,* playing an
497 important role in virulence regulation, biofilm development, natural transformation,
498 and stress response [42]. By means of sequence alignments we identified sequences
499 characteristic of the HapR-binding motif 1 in front of *metT*, *msrC*, *metI*, and a HapR-
500 binding motif 2-like sequence in front of *metR* (Fig. 4H). Indeed, HapR directly
501 promotes the transcription of these four genes, as demonstrated by RT-qPCR (Fig. 4I),
502 and binding of HapR to promoter DNA was demonstrated by EMSA experiments (Fig. 4J,
503 Supplementary Fig. S13). We observed that it rescued the growth defect of Δ*flaA* in
504 methionine-limited medium (MM) (Fig. 4K) and adding methionine to the medium did
505 not revive the growth of Δ*flhB*Δ*metR*Δ*msrC*Δ*metI*Δ*metT* (Fig. 4L).

506 *3.6 Methionine metabolism affects V. cholerae colonization*

507 To examine the metabolic activity of Δ*flhB*, Δ*flaA* and WT in vitro, we used FITC-
508 labeled glucose method (Fig. 5A). The metabolic activity is often labeled by marking
509 bacterial cell wall precursors [50, 51], such as GlcNAc-1-phosphate, which is originally
510 derived from glucose [52]. Fluorescein Isothiocyanate (FITC) is a commonly used
511 fluorescent probe molecule that can form a covalent complex with glucose molecules.
512 After FITC-labeled glucose is utilized, the detection of fluorescence signals can
513 indicate bacterial metabolic activity. A transwell co-culture system with WT showed
514 that the population of Δ*flhB* was highly metabolically active and 1.7-fold higher than
515 WT (P=0.012), while Δ*flaA* was 0.6-fold lower (P=0.003) than WT (Fig. 5B). We also
516 investigated bacterial metabolism in vivo by administering FITC-labeled glucose to
517 mice that were colonized with either a Δ*flaA* and WT mixture or a Δ*flhB* and WT
518 mixture, after which the bacterial content was isolated from their intestine and subjected
519 to flow cytometry to sort those bacterial cells with high metabolic activity. These were
520 enumerated on X-Gal plates, which revealed that the population of Δ*flhB* was 7-fold
521 higher (P=0.017), while the population of Δ*flaA* was 0.2-fold lower compared to WT
522 (P=0.001) (Fig. 5C). Thus, both in vitro co-culture and in vivo in adult mice co-
523 colonization experiments provided strong evidence that bacterial metabolic activity
524 contributed benefited the bacteria. In combination with the other results, this suggest
525 that differences in methionine-related metabolic activity may contribute to the different
526 colonization patterns of the flagellar mutants.

527 *3.7 Ecological simulation of flagellar mutants reveals trade-off mechanisms between*
528 *motility loss and host adaptability.*

529 To assess the host adaptability of the flagellar mutants, the previously characterized
530 mutants were labeled using a novelty developed 6N-labeling method and subsequently
531 administered to adult mice via oral gavage. Colonization competition was then assessed
532 by high-throughput sequencing (Fig. 5D, Table S8). In the absence of methionine
533 supplementation, the competition indices (CIs) of all 26 mutants showed a scattered
534 and diverse distribution, consistent with the head-to-head colonization outcomes
535 presented earlier (Fig. 2B). Upon methionine addition, the distribution of CIs for all
536 flagellar mutants became markedly more constrained, as detailed in Supplementary
537 Dataset 6. Further pairwise analysis revealed that methionine supplementation could
538 reverse the colonization pattern of individual flagellar mutants (Fig. 5E). Collectively,
539 these findings demonstrate that ecological simulation of flagellar mutants reveals trade-
540 off mechanisms between motility loss and host adaptability.

541 ***4. Discussion***

542 By employing big data analysis on *V. cholerae* life cycle samples, this study
543 elucidates the trade-off mechanism whereby flagellar mutations result in motility loss

544 yet enhance host adaptability through the FlgM-FliA-HapR-methionine axis, a driver
545 of metabolic reprogramming (Fig. 6).

546 Although flagellar mutations are prevalent across the life cycle environments of *V.*
547 *cholerae*, their evolutionary paths across distinct host niches remain unclear. Previous
548 work indicates that the cyclin gene *dps*, rather than DNA repair or ROS/RNS
549 scavenging systems, significantly increases flagellar mutation frequency in an adult
550 mouse model [15]. In amoeba hosts, mutations in the transcriptional
551 regulator *flrA* provide a competitive edge, while intense microbial competition in the
552 gut may further shape *V. cholerae* evolution [16]. In addition, the *flrA* in *V.*
553 *cholerae* senses intracellular levels of the second messenger cyclic diguanylate
554 monophosphate (c-di-GMP) in response to dietary signals. Under a high c-di-GMP
555 environment induced by casein, FlrA represses the expression of the type VI secretion
556 system (T6SS), thereby impairing the ability of *V. cholerae* to compete with intestinal
557 commensal bacteria via T6SS and ultimately leading to a colonization defect in casein-
558 fed mice [53]. Furthermore, intense microbial competition in the gut may serve as a
559 major driving force for the evolution of *V. cholerae* within the intestinal environment
560 [54]. Integrating comparative genomics with experimental evolution assays may
561 unravel whether these mutations represent adaptations to host niches or collateral
562 effects of pathogen transmission dynamics.

563 Methionine is an essential amino acid utilized by bacteria in various physiological
564 and metabolic processes, including polyamine synthesis, DNA synthesis, redox balance,
565 and DNA and histone methylation [55]. Also, it is important to note that methionine
566 plays an essential role in the immune system through its metabolites. For example, in
567 response to antigens, T cells activate the methionine cycle to support proliferation and
568 differentiation in cancer, indicating the importance of the methionine cycle to T cell
569 immunity [56]. Methionine supplementation or restriction can intervene in the natural
570 antioxidant capacity of an organism by leading to the production of endogenous
571 enzymes that reduce oxidative stress and DNA damage [57]. These data imply that *V.*
572 *cholerae* may employ the methionine pathway as a means of immune evasion. To
573 successfully propagate and cause disease, *V. cholerae* also evades the immune system
574 by repressing the mannose-sensitive hemagglutinin pilus via the transcription factor
575 ToxT, preventing secretory IgA binding and enabling intestinal colonization to bypass
576 host defenses [58].

577 Methionine metabolism is a central node within the interconnected amino acid
578 network of *V. cholerae* [59]. Beyond its metabolic functions, methionine serves as a
579 precursor for S-adenosylmethionine (SAM), a cofactor involved in critical processes
580 including the synthesis of the quorum-sensing autoinducer CAI-1 [60,61]. Similarly,
581 threonine, another methionine-derived metabolite, may contribute to autoinducer DPO
582 synthesis, and in *Pseudomonas aeruginosa*, SAM participates in producing AI-1, AI-2,
583 and AHLs [62]. Analyzing methionine flux could therefore help identify key

584 metabolites that enhance colonization in flagellar mutants, and future work should
585 examine whether intermediate methionine metabolites or other amino acids influence *V.*
586 *cholerae* colonization through bacterial or host metabolic remodeling.

587 This study found that HapR binds to promoters of methionine metabolism-related
588 genes (*metR*, *msrC*, *metI*, *metT*), a result not reported in prior systematic screens of
589 HapR targets. The discrepancy may stem from limitations in bioinformatic prediction
590 accuracy and variability in HapR-binding sequences [42]. Beyond methionine
591 regulation, HapR suppresses toxin-coregulated pilus (TCP) and cholera toxin (CTX)
592 genes by repressing *aphA*, while activating extracellular proteases and modulating
593 T6SS genes [63-65]. However, in adult and infant mouse models, this virulence factors
594 do not substantially affect colonization [39,66]. HapR also inhibits biofilm formation
595 via cyclic di-GMP modulation and *vpsT* repression [67-69], although flagellar mutants
596 show enhanced biofilm capacity, they still exhibit colonization defects, indicating
597 biofilm is not a major driver of colonization in these strains. Additionally, HapR and
598 RpoS jointly facilitate stress adaptation, luminal dispersal, and host exit. Although the
599 flagellar mutants of *V. cholerae* exhibit enhanced biofilm formation capacity, they still
600 display a colonization defect (Supplementary Fig. S3, Fig. 2B), suggesting that biofilm
601 formation is also not a major factor contributing to enhanced colonization in these
602 mutants. In addition, HapR and RpoS collectively facilitates stress adaptation to host
603 factors, dispersal within the intestinal lumen, and eventual exit of *V. cholerae* from the
604 host [70]. In the precipitated proteome, we observed that MsrC was the most highly
605 enriched cellular protein in Δ*flhB* (Log2Ratio = 3.000, P = 0.002) relative to Δ*flaA* (Fig.
606 4A). Through experimental validation, we concluded that methionine contributes to the
607 differential colonization patterns among the 26 flagellar mutants in adult mice.
608 The flagellum renders bacteria motility, but it is also a major antigen recognized by
609 the host [71, 72]. Extensive studies have shown that flagellar mutants of *V. cholerae*
610 are frequently present in clinical and environmental samples, and specifically the *V.*
611 *cholerae* Haiti strains contain multiple mutational hotspots in flagellum gene regions
612 according to SNP analysis [11]. Besides mutations, *V. cholerae* also actively loses
613 flagellar filaments during environmental changes such as mucus penetration [4],
614 biofilm development [10], and host Lypd8 promotes the segregation antibody capture
615 [72]. This is also demonstrated for other pathogenic bacteria. The freshwater bacterium
616 *Caulobacter crescentus* loses its flagella through ejection trigged by ClpA [73]. The
617 loss of the polar flagellum in *V. fischeri* and in plant-associated *Methylobacteria* has
618 also been reported [74, 75]. Bacterial flagella also detach during starvation [76].
619 We demonstrated that the trade-off mechanism between motility loss and host
620 adaptability operates via the sophisticated FlgM-FliA-HapR-methionine metabolic
621 reprogramming axis. However, this study has the following limitations: (1) The
622 mechanistic focus on the FlgM-FliA-HapR-methionine axis, though insightful, may not
623 capture the full complexity of the flagellar regulatory network, and deeper metabolic
624 validation is needed; (2) It does not directly simulate or verify how this trade-off
625 process dynamically occurs and becomes fixed within a population under

environmental pressure, lacking direct experimental evolution evidence in human; (3) The adaptive efficacy and stability of the revealed mechanism in such highly complex real-world environments require further evaluation; (4) Time-course experiments were not provided to track the changes in FlgM secretion, HapR expression, and methionine metabolism over the course of infection.

4. Conclusion

Based on extensive sample analysis, this study reveals that flagellar mutations in *V. cholerae* cluster in key structural and regulatory genes, underscoring their central role in host adaptation. Specifically, the secretion level of the flagellar regulator FlgM drives a phenotypic shift from motility to host adaptability. This transition is mediated through the FlgM-FliA-HapR-methionine axis, which balances the loss of motility with enhanced host adaptability. Ultimately, impaired motility promotes environmental fitness by activating quorum sensing and reprogramming methionine metabolism, elucidating a novel evolutionary trade-off strategy between movement and adaptability at the molecular level.

Environmental implications

V. cholerae can persist in both aquatic environments and the human intestinal tract, posing substantial impacts on environmental and human health. Genetic mutations enable the bacterium to survive under complex environmental stresses, thereby increasing the risk of human infection. This study demonstrates that *V. cholerae* can acquire flagellar gene mutations across different environmental niches within its life cycle. Notably, mutations in key genes enhance its adaptability within the host intestine, a process mediated by the FlgM-FliA-HapR-methionine metabolic axis. Our findings elucidate the trade-off mechanism between motility loss and host adaptability, offering novel perspectives on bacterial evolution and pathogenicity.

CRediT authorship contribution statement

Guozhong Chen: Conceptualization, Methodology, Investigation, Project administration, Funding acquisition, Visualization, Writing-original draft, Writing-review & editing. **Zixin Qin:** Methodology, Investigation, Visualization. **Fenxia Fan:** Investigation, Writing-review & editing, Funding acquisition. **Mei Luo:** Writing-review & editing. **Hongou Wang:** Methodology. **Baoshuai Xue:** Methodology. **Shucheng Li:** Methodology. **Shiyong Chen:** Supervision. **Xiaoman Yang:** Investigation. **Xiang Mao:** Investigation. **Liwen Yi:** Investigation. **Chunrong Yi:** Investigation. **Wei Li:** Investigation, Supervision. **Xiaoyun Liu:** Project administration, Funding acquisition. **Biao Kan:** Supervision, Project administration. **Zhi Liu:** Conceptualization, Methodology, Visualization, Project administration, Funding acquisition, Supervision, Writing-original draft, Writing-review & editing.

Declaration of Competing Interest

The authors declare no financial/commercial conflicts of interests.

Acknowledgments

We are grateful to all the members of our team. We thank Core Facilities for Life Science, Huazhong University of Science and Technology for the technical support. We also thank Core Facilities for Life and Environmental Sciences, State Key laboratory of Microbial Technology of Shandong University for technical guidance. This study was supported by National Natural Science Foundation of China under the grant numbers 31770132 (to Z. L), (22174003 and 21974002 to X. Y. L) and National Key Research and Development Program of China (2022YFA1304500 to X. Y. L), National Key Research and Development Program of China (2021YFC2300304 to F. X. F), Shandong Province Science Foundation for Youths (ZR2024QC312 to G. Z. C).

Supplementary Material

Supplementary material is available online.

Data Availability

The proteomic data that support the findings of this study are openly available in the iProX database at https://www.iprox.cn//page/SCV017.html?query=IPX0005998000, accession number IPX0005998000. The raw data of 6N-Label is openly available in the NCBI database at https://www.ncbi.nlm.nih.gov/sra/?term=PRJNA1099378, reference number PRJNA1099378. The codes for 6N-Label relative abundance analysis, bins acquisition and species annotation from cohort-based studies, and analyzing high-frequency mutations in the flagellar genes of *V. cholerae* of this study are openly available in Zenodo at https://doi.org/10.5281/zenodo.14920964, reference number 14920964.

References

1. Kanungo S, Azman AS, Ramamurthy T, Deen J, Dutta S. Cholera. *Lancet* 2022; **399**: 1429-1440. https://doi.org/10.1016/s0140-6736(22)00330-0.
2. World Health Organization. Cholera. https://www.who.int/news-room/fact-sheets/detail/cholera (10 February 2025, date last accessed).
3. D. Chac, C. N. Dunmire, J. Singh, A. A. Weil. Update on environmental and hostfactors impacting the risk of *Vibrio cholerae* infection. ACS Infectious Diseases,2021, 7(5): 1010-1019. https://doi.org/10.1021/acsinfecdis.0c00914.
4. Liu Z, Miyashiro T, Tsou A, Hsiao A, Goulian M, Zhu J. Mucosal penetration primes *Vibrio cholerae* for host colonization by repressing quorum sensing. *Proc Natl Acad Sci U S A* 2008; **105**: 9769-9774. https://doi.org/10.1073/pnas.0802241105.

699 5. Echazarreta MA, Klose KE. *Vibrio* flagellar synthesis. Front Cell Infect Microbiol
700 2019; 9: 131. https://doi.org/10.3389/fcimb.2019.00131.
701 6. Syed KA, Beyhan S, Correa N, Queen J, Liu J, Peng F, et al. The *Vibrio cholerae*
702 flagellar regulatory hierarchy controls expression of virulence factors. *J Bacteriol*
703 2009; **191**: 6555–6570. https://doi.org/10.1128/jb.00949-09.
704 7. Sowa Y, Berry RM. Bacterial flagellar motor. *Q Rev Biophys* 2008; **41**: 103-132.
705 https://doi.org/10.1017/s0033583508004691.
706 8. Attridge SR, Rowley D. The role of the flagellum in the adherence of *Vibrio*
707 *cholerae*. *J Infect Dis* 1983; **147**: 864-872.
708 https://doi.org/10.1093/infdis/147.5.864.
709 9. Butler SM, Camilli A. Both chemotaxis and net motility greatly influence the
710 infectivity of *Vibrio cholerae*. *Proc Natl Acad Sci U S A* 2004; **101**: 5018-5023.
711 https://doi.org/10.1073/pnas.0308052101.
712 10. Wu DC, Zamorano-Sánchez D, Pagliai FA, Park JH, Floyd KA, Lee CK, et al.
713 Reciprocal c-di-GMP signaling: Incomplete flagellum biogenesis triggers c-di-
714 GMP signaling pathways that promote biofilm formation. *PLoS Genet* 2020; **16**:
715 e1008703. https://doi.org/10.1371/journal.pgen.1008703.
716 11. Katz LS, Petkau A, Beaulaurier J, Tyler S, Antonova ES, Turnsek MA, et al.
717 Evolutionary dynamics of *Vibrio cholerae* O1 following a single-source
718 introduction to Haiti. *mBio* 2013; **4**: 1-10. https://doi.org/10.1128/mbio.00398-13.
719 12. Mostow P, Richardson K. High-frequency spontaneous mutation of classical
720 *Vibrio cholerae* to a nonmotile phenotype. *Infect Immun* 1990; **58**: 3633-3639.
721 https://doi.org/10.1128/iai.58.11.3633-3639.1990.
722 13. Jubair M, Atanasova KR, Rahman M, Klose KE, Yasmin M, Yilmaz O, et al.
723 *Vibrio cholerae* persisted in microcosm for 700 days inhibits motility but promotes
724 biofilm formation in nutrient-poor lake water microcosms. *PLoS One* 2014; **9**:
725 e92883. https://doi.org/10.1371/journal.pone.0092883.
726 14. Giacomucci S, Mathieu-Denoncourt A, Vincent AT, Jannadi H, Duperthuy M.
727 Experimental evolution of *Vibrio cholerae* identifies hypervesiculation as a way to
728 increase motility in the presence of polymyxin B. *Front Microbiol* 2022; **13**: 1-18.
729 https://doi.org/10.3389/fmicb.2022.932165.
730 15. Hoque MM, Noorian P, Espinoza-Vergara G, Manuneedhi Cholan P, Kim M,
731 Rahman MH, et al. Adaptation to an amoeba host drives selection of virulence-
732 associated traits in *Vibrio cholerae*. *ISME J* 2022; **16**: 856-867.
733 https://doi.org/10.1038/s41396-021-01134-2.
734 16. Luo M, Chen G, Yi C, Xue B, Yang X, Ma Y, et al. Dps-dependent in vivo
735 mutation enhances long-term host adaptation in *Vibrio cholerae*. *PLoS Pathog*
736 2023; **19**: e1011250. https://doi.org/10.1371/journal.ppat.1011250.
737 17. Klose KE, Mekalanos JJ. Distinct roles of an alternative sigma factor during both
738 free-swimming and colonizing phases of the *Vibrio cholerae* pathogenic cycle.
739 *Mol Microbiol* 1998; **28**: 501-520. https://doi.org/10.1046/j.1365-
740 2958.1998.00809.x.

741 18. Azarian T, Ali A, Johnson JA, Mohr D, Prosperi M, Veras NM, et al.
742 Phylodynamic analysis of clinical and environmental *Vibrio cholerae* isolates from
743 Haiti reveals diversification driven by positive selection. *mBio* 2014; **5**: e01824-
744 14. https://doi.org/10.1128/mbio.01824-14.
745 19. Daboul J, Weghorst L, DeAngelis C, Plecha SC, Saul-McBeth J, Matson JS.
746 Characterization of *Vibrio cholerae* isolates from freshwater sources in northwest
747 Ohio. *PLoS One* 2020; **15**: e0238438.
748 https://doi.org/10.1371/journal.pone.0238438.
749 20. Mavian C, Paisie TK, Alam MT, Browne C, de Rochars VMB, Nembrini S, et al.
750 Toxigenic *Vibrio cholerae* evolution and establishment of reservoirs in aquatic
751 ecosystems. *Proc Natl Acad Sci U S A* 2020; **117**: 7897-7904.
752 https://doi.org/10.1073/pnas.1918763117.
753 21. Mwaba J, Debes AK, Murt KN, Shea P, Simuyandi M, Laban N, et al. Three
754 transmission events of *Vibrio cholerae* O1 into Lusaka, Zambia. *BMC Infect Dis*
755 2021; **21**: 570. https://doi.org/10.1186/s12879-021-06259-5.
756 22. Chen, Shifu. Ultrafast one-pass FASTQ data preprocessing, quality control, and
757 deduplication using fastp. *iMeta* 2023; **2**: 1-5. https://doi.org/10.1002/imt2.107.
758 23. Uritskiy, Gherman V., DiRuggiero Jocelyne, Taylor James. MetaWRAP—a
759 flexible pipeline for genome-resolved metagenomic data analysis. *Microbiome*
760 2018; **6**: 158. https://doi.org/10.1186/s40168-018-0541-1.
761 24. Chaumeil, Pierre-Alain, Mussig Aaron J, Hugenholtz Philip, Parks Donovan H.
762 GTDB-Tk v2: memory friendly classification with the genome taxonomy database.
763 *Bioinformatics* 2022; **38**: 5315-5316.
764 https://doi.org/10.1093/bioinformatics/btac672.
765 25. Hyatt, Doug, Chen Gwo-liang, LoCascio Philip F, Land Miriam L, Larimer Frank
766 W, Hauser Loren J. Prodigal: Prokaryotic gene recognition and translation
767 initiation site identification. *BMC Bioinformatics* 2010; **11**:119.
768 https://doi.org/10.1186/1471-2105-11-119.
769 26. Buchfink, B., Xie, C. & Huson, D. H. Fast and sensitive protein alignment using
770 DIAMOND. Nature Methods 2015;**12**: 59-60. https://doi.org/10.1038/nmeth.3176
771 27. Farhadi T, Nezafat N, Ghasemi Y. In silico phylogenetic analysis of *Vibrio*
772 *cholerae* isolates based on three housekeeping genes. Int J Comput Biol Drug Des.
773 2015;8(1):62-74. https://doi.org/10.1504/ijcbdd.2015.068789
774 28. Rui YY, Kan B, Gao SY, Liu YQ, Qi GM. Sequence analysis of housekeeping
775 genes *recA*, *dnaE*, and *mdh* in different serogroups or biotypes of *Vibrio cholerae*
776 isolated from China. Nan Fang Yi Ke Da Xue Xue Bao. 2006;26(12):1720-1723.
777 https://www.j-smu.com/CN/Y2006/V26/I12/1720
778 29. Houot L, Watnick PI. A novel role for enzyme I of the *Vibrio cholerae*
779 phosphoenolpyruvate phosphotransferase system in regulation of growth in a
780 biofilm. *J Bacteriol* 2008; **190**: 311-320. https://doi.org/10.1128/jb.01410-07.
781 30. Metcalf WW, Jiang W, Daniels LL, Kim SK, Haldimann A, Wanner BL.
782 Conditionally replicative and conjugative plasmids carrying lacZα for cloning,

783 mutagenesis, and allele replacement in bacteria. *Plasmid* 1996; **35**: 1-13.
784 https://doi.org/10.1006/plas.1996.0001.
785 31. Xia A, Qian M, Wang C, Huang Y, Liu Z, Ni L, et al. Optogenetic modification of
786 *Pseudomonas aeruginosa* enables controllable twitching motility and host
787 infection. *ACS Synth Biol* 2021; **10**: 531-541.
788 https://doi.org/10.1021/acssynbio.0c00559.
789 32. Ma Y, Yang X, Wang H, Qin Z, Yi C, Shi C, et al. CBS-derived H_2S facilitates
790 host colonization of *Vibrio cholerae* by promoting the iron-dependent catalase
791 activity of KatB. *PLoS Pathog* 2021; **17**: e1009763.
792 https://doi.org/10.1371/journal.ppat.1009763.
793 33. Liu Z, Wang H, Zhou Z, Sheng Y, Naseer N, Kan B, et al. Thiol-based switch
794 mechanism of virulence regulator AphB modulates oxidative stress response in
795 *Vibrio cholerae*. *Mol Microbiol* 2016; **102**: 939-949.
796 https://doi.org/10.1111/mmi.13524.
797 34. Hong S, Zheng DW, Zhang QL, Deng WW, Song WF, Cheng SX, et al. An RGB-
798 emitting molecular cocktail for the detection of bacterial fingerprints. *Chem Sci*
799 2020; **11**: 4403-4409. https://doi.org/10.1039/d0sc01704c.
800 35. Lin L, Song J, Du Y, Wu Q, Gao J, Song Y, et al. Quantification of bacterial
801 metabolic activities in the gut by d-Amino acid-based in vivo labeling. *Angew*
802 *Chemie - Int Ed* 2020; **59**: 11923-11926. https://doi.org/10.1002/anie.202004703.
803 36. Dalia AB, McDonough EK, Camilli A. Multiplex genome editing by natural
804 transformation. *Proc Natl Acad Sci U S A* 2014; **111**: 8937-8942.
805 https://doi.org/10.1073/pnas.1406478111.
806 37. Hoque MM, Noorian P, Espinoza-Vergara G, Manuneedhi Cholan P, Kim M,
807 Rahman MH, et al. Adaptation to an amoeba host drives selection of virulence-
808 associated traits in *Vibrio cholerae*. *ISME J* 2022; 16: 856-867.
809 https://doi.org/10.1038/s41396-021-01134-2.
810 38. Martinez RM, Dharmasena MN, Kirn TJ, Taylor RK. Characterization of two outer
811 membrane proteins, FlgO and FlgP, that influence *Vibrio cholerae* motility. *J*
812 *Bacteriol* 2009; **191**: 5669-5679. https://doi.org/10.1128/jb.00632-09.
813 39. Olivier V, Salzman NH, Satchell KJF. Prolonged Colonization of Mice by *Vibrio*
814 *cholerae* El Tor O1 Depends on Accessory Toxins. *Infect Immun* 2007; **75**: 5043-
815 5051. https://doi.org/10.1128/iai.00508-07.
816 40. Correa NE, Barker JR, Klose KE. The *Vibrio cholerae* FlgM homologue is an anti-
817 σ^{28} factor that is secreted through the sheathed polar flagellum. *J Bacteriol* 2004;
818 **186**: 4613-4619. https://doi.org/10.1128/jb.186.14.4613-4619.2004.
819 41. Qin Z, Yang X, Chen G, Park C, Liu Z. Crosstalks between gut microbiota and
820 *Vibrio cholerae*. *Front Cell Infect Microbiol* 2020; **10**: 582554.
821 https://doi.org/10.3389/fcimb.2020.582554.
822 42. Tsou AM, Cai T, Liu Z, Zhu J, Kulkarni R V. Regulatory targets of quorum sensing
823 in *Vibrio cholerae*: Evidence for two distinct HapR-binding motifs. *Nucleic Acids*
824 *Res* 2009; **37**: 2747-2756. https://doi.org/10.1093/nar/gkp121.

825 43. Tsou AM, Liu Z, Cai T, Zhu J. The VarS/VarA two-component system modulates
826 the activity of the *Vibrio cholerae* quorum-sensing transcriptional regulator HapR.
827 *Microbiology* 2011; **157**: 1620-1628. https://doi.org/10.1099/mic.0.046235-0.
828 44. Herzog R, Peschek N, Fröhlich KS, Schumacher K, Papenfort K. Three
829 autoinducer molecules act in concert to control virulence gene expression in *Vibrio*
830 *cholerae*. *Nucleic Acids Res* 2019; **47**: 3171-3183.
831 https://doi.org/10.1093/nar/gky1320.
832 45. Liu Z, Hsiao A, Joelsson A, Zhu J. The transcriptional regulator VqmA increases
833 expression of the quorum-sensing activator HapR in *Vibrio cholerae*. *J Bacteriol*
834 2006; **188**: 2446-2453. https://doi.org/10.1128/jb.188.7.2446-2453.2006
835 46. Vanhove AS, Jugder BE, Barraza D, Watnick PI. Methionine availability in the
836 arthropod intestine is elucidated through identification of *Vibrio cholerae*
837 methionine acquisition systems. *Appl Environ Microbiol* 2020; **86**: e00371-20.
838 https://doi.org/10.1128/aem.00371-20.
839 47. Kanehisa M. KEGG: Kyoto Encyclopedia of Genes and Genomes. *Nucleic Acids*
840 *Res* 2000; **28**: 27-30. https://doi.org/10.1093/nar/28.1.27.
841 48. Zhang Z, Chen G, Hu J, Hussain W, Fan F, Yang Y, et al. Mr.Vc: A database of
842 microarray and RNA-seq of *Vibrio cholerae*. *Database* 2019; **2019**: 1-8.
843 https://doi.org/10.1093/database/baz069.
844 49. Zhang Z, Chen G, Hussain W, Qin Z, Liu J, Su Y, et al. Mr.Vc v2: An updated
845 version of database with increased data of transcriptome and experimental
846 validated interactions. *Front Microbiol* 2022; **13**: 1047259.
847 https://doi.org/10.3389/fmicb.2022.1047259.
848 50. Calabretta PJ, Hodges HL, Kraft MB, Marando VM, Kiessling LL. Bacterial cell
849 wall modification with a glycolipid substrate. *J Am Chem Soc* 2019; **141**: 9262-
850 9272. https://doi.org/10.1021/jacs.9b02290.
851 51. Xu Y, Hernández-Rocamora VM, Lorent JH, Cox R, Wang X, Bao X, et al.
852 Metabolic labeling of the bacterial peptidoglycan by functionalized glucosamine.
853 *iScience* 2022; **25**: 104753. https://doi.org/10.1016/j.isci.2022.104753.
854 52. Sadamoto R, Matsubayashi T, Shimizu M, Ueda T, Koshida S, Koda T, et al.
855 Bacterial surface engineering utilizing glucosamine phosphate derivatives as cell
856 wall precursor surrogates. *Chem - A Eur J* 2008; **14**: 10192-10195.
857 https://doi.org/10.1002/chem.200801734.
858 53. Liu, R. et al. Diet modulates *Vibrio cholerae* colonization and competitive
859 outcomes with the gut microbiota. *Cell Host and Microbe* 2025; **33**, 2085-2099.e5.
860 https://doi.org/10.1016/j.chom.2025.11.004.
861 54. Jiang S, Zhang C, Han Z, Ma W, Wang S, Huo D, Cui W, Zhai Q, Huang S, Zhang
862 J. Native microbiome dominates over host factors in shaping the probiotic genetic
863 evolution in the gut. *NPJ Biofilms Microbiomes*. 2023; 1:80.
864 https://doi.org/10.1038/s41522-023-00447-8.

865 55. Martínez Y, Li X, Liu G, Bin P, Yan W, Más D, et al. The role of methionine on
866 metabolism, oxidative stress, and diseases. *Amino Acids* 2017; **49**: 2091-2098.
867 https://doi.org/10.1007/s00726-017-2494-2.
868 56. Zhao T, Lum JJ. Methionine cycle-dependent regulation of T cells in cancer
869 immunity. *Front Oncol* 2022; **12**: 1-9. https://doi.org/10.3389/fonc.2022.969563.
870 57. Martínez Y, Li X, Liu G, Bin P, Yan W, Más D, et al. The role of methionine on
871 metabolism, oxidative stress, and diseases. *Amino Acids* 2017; **49**: 2091-2098.
872 https://doi.org/10.1007/s00726-017-2494-2.
873 58. Hsiao A, Liu Z, Joelsson A, Zhu J. *Vibrio cholerae* virulence regulator-coordinated
874 evasion of host immunity. *Proc Natl Acad Sci U S A* 2006; **103**: 14542-14547.
875 https://doi.org/10.1073/pnas.0604650103.
876 59. Bogard RW, Davies BW, Mekalanos JJ. MetR-regulated *Vibrio cholerae*
877 metabolism is required for virulence. *mBio* 2012; **3**.e00236-12.
878 https://doi.org/10.1128/mbio.00236-12.
879 60. Hondorp ER, Matthews RG. Methionine. *EcoSal Plus* 2006; **2**: 185-185.
880 https://doi.org/10.1128/ecosalplus.3.6.1.7.
881 61. Winans SC. A new family of quorum sensing pheromones synthesized using S-
882 adenosylmethionine and Acyl-CoAs. *Mol Microbiol* 2011; **79**: 1403-1406.
883 https://doi.org/10.1111/j.1365-2958.2011.07551.x.
884 62. Heurlier, K., Dénervaud, V. & Haas, D. Impact of quorum sensing on fitness of
885 *Pseudomonas aeruginosa*. *International Journal of Medical Microbiology* 2006,
886 **296**, 93-102. https://doi.org/10.1016/j.ijmm.2006.01.043.
887 63. Cho JY, Liu R, Macbeth JC, Hsiao A. The interface of *Vibrio cholerae* and the gut
888 microbiome. *Gut Microbes*. 2021, 13:1937015.
889 https://doi.org/10.1080/19490976.2021.1937015.
890 64. 2. Hsiao A, Zhu J. Pathogenicity and virulence regulation of *Vibrio cholerae* at the
891 interface of host-gut microbiome interactions. *Virulence*. 2020; **11**:1582-1599.
892 https://doi.org/10.1080/21505594.2020.1845039.
893 65. 3. Qin Z, Yang X, Chen G, Park C, Liu Z. Crosstalks between gut microbiota and
894 *Vibrio cholerae*. *Front Cell Infect Microbiol* 2020; **10**: 582554.
895 https://doi.org/10.3389/fcimb.2020.582554.
896 66. Silva AJ, Leitch GJ, Camilli A, Benitez JA. Contribution of
897 hemagglutinin/protease and motility to the pathogenesis of El Tor biotype cholera.
898 *Infect Immun*. 2006;**74**:2072-9. https://doi.org/10.1128/iai.74.4.2072-2079.2006.
899 67. Waters CM, Lu W, Rabinowitz JD, Bassler BL. Quorum sensing controls biofilm
900 formation in *Vibrio cholerae* through modulation of cyclic di-GMP levels and
901 repression of *vpsT*. *J Bacteriol*. 2008; **190**:2527-36.
902 https://doi.org/10.1128/jb.01756-07
903 68. Srivastava D, Harris RC, Waters CM. Integration of cyclic di-GMP and quorum
904 sensing in the control of *vpsT* and *aphA* in *Vibrio cholerae*. *J Bacteriol*. 2011
905 Nov;193(22):6331-41. https://doi.org/10.1128/jb.05167-11

69. Johnson GE, Fei C, Wingreen NS, Bassler BL. Analysis of gene expression within individual cells reveals spatiotemporal patterns underlying *Vibrio cholerae* biofilm development. *PLoS Biol*. 2025; **23**: e3003187. https://doi.org/10.1371/journal.pbio.3003187
70. Joelsson A, Kan B, Zhu J. Quorum sensing enhances the stress response in *Vibrio cholerae*. *Appl Environ Microbiol*. 2007; **73**:3742-6. https://doi.org/10.1128/aem.02804-06.
71. Khan F, Tabassum N, Anand R, Kim YM. Motility of *Vibrio* spp.: regulation and controlling strategies. *Appl Microbiol Biotechnol* 2020; **104**: 8187-8208. https://doi.org/10.1007/s00253-020-10794-7.
72. Okumura R, Kurakawa T, Nakano T, Kayama H, Kinoshita M, Motooka D, et al. Lypd8 promotes the segregation of flagellated microbiota and colonic epithelia. *Nature* 2016; **532**: 117-121. https://doi.org/10.1038/nature17406.
73. Grünenfelder B, Tawfilis S, Gehrig S, Østerås M, Eglin D, Jenal U. Identification of the protease and the turnover signal responsible for cell cycle-dependent degradation of the Caulobacter FliF motor protein. *J Bacteriol* 2004; **186**: 4960-4971. https://doi.org/10.1128/jb.186.15.4960-4971.2004.
74. Ruby EG, Asato LM. Growth and flagellation of *Vibrio fischeri* during initiation of the sepiolid squid light organ symbiosis. *Arch Microbiol* 1993; **159**: 160-167. https://doi.org/10.1007/bf00250277.
75. Doerges L, Kutschera U. Assembly and loss of the polar flagellum in plant-associated methylobacteria. *Naturwissenschaften* 2014; **101**: 339-346. https://doi.org/10.1007/s00114-014-1162-6.
76. Zhu S, Gao B. Bacterial flagella loss under starvation. *Trends Microbiol* 2020; **28**: 785-788. https://doi.org/10.1016/j.tim.2020.05.002.

Figures and Tables

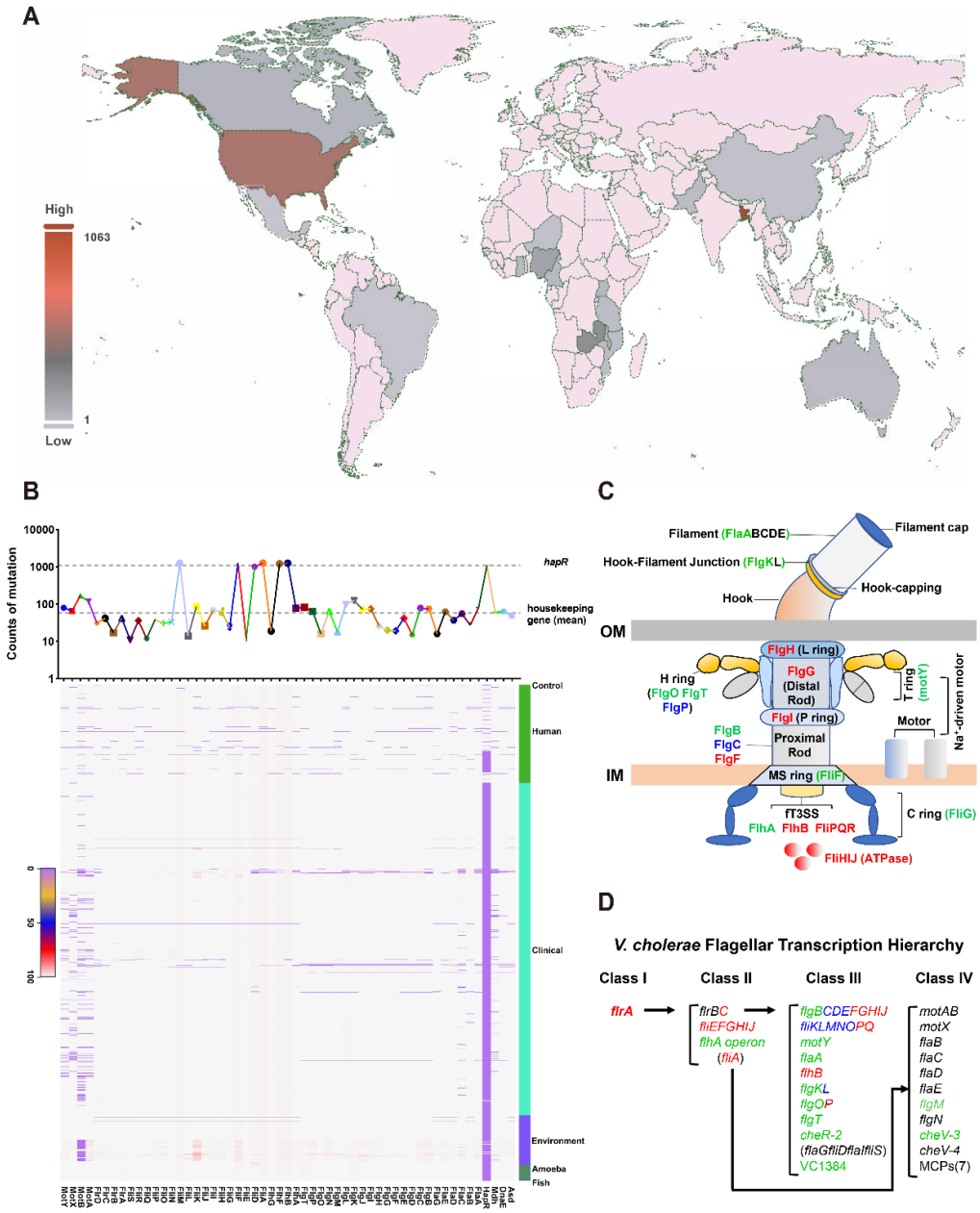

Fig. 1. High-frequency mutations in the flagellar genes of *V. cholerae* from the life cycle. (**A**), World distribution map of the collected samples, with areas in pink indicating no sample collection. (**B**) Spectrum and count statistics of flagellar gene mutations. The *hapR* and housekeeping genes (*asd*, *dnaE*, *mdh*) were used as controls. (**C**) Schematic diagram of the *V. cholerae* flagellum assembly. (**D**) *V. cholerae* flagellar transcription hierarchy.

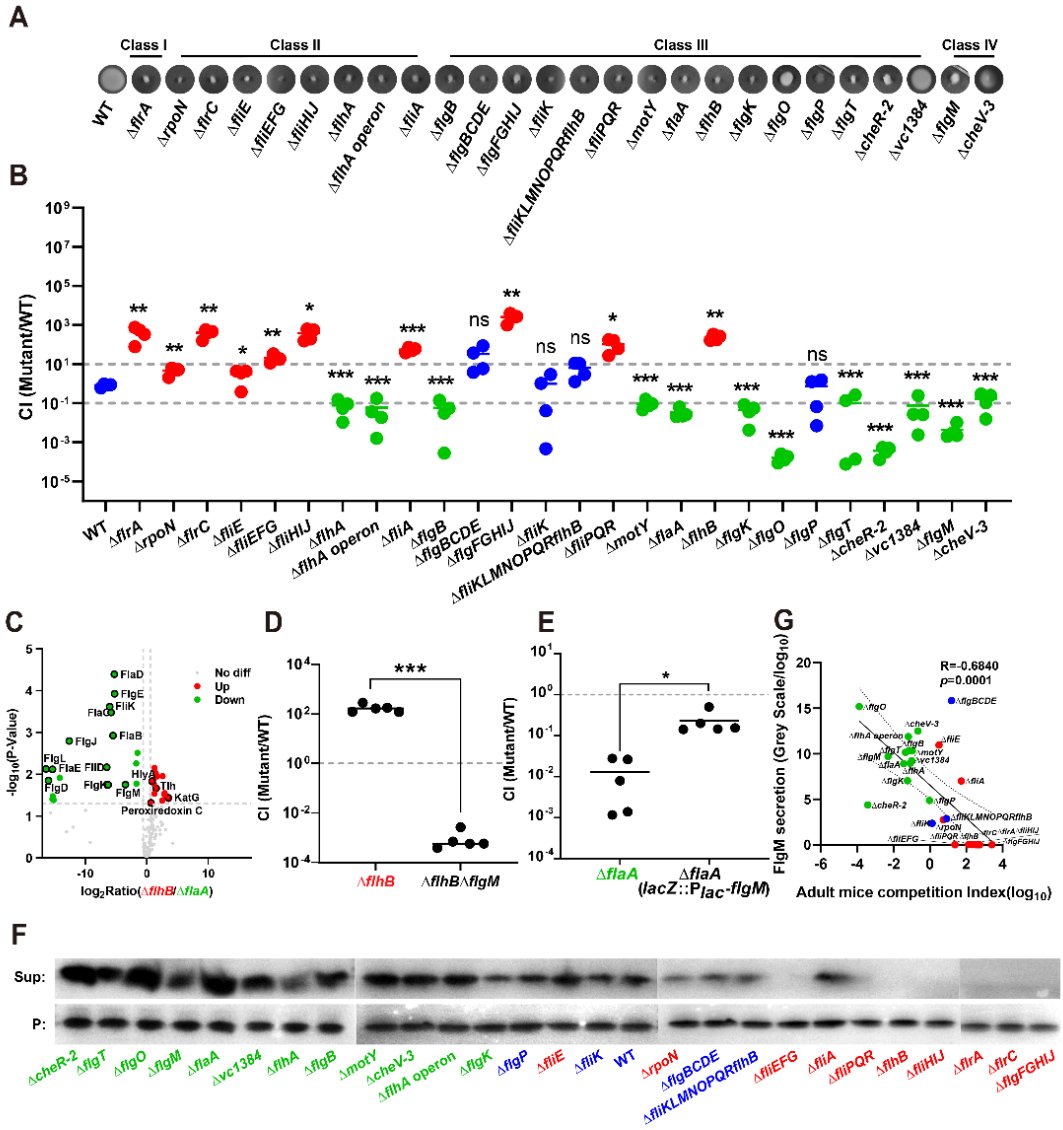

Fig. 2. FlgM secretion regulates colonization of *V. cholerae* flagellar mutants. (**A**), Motility assay. (**B**), Competition assay in adult mice. The horizontal bar indicates the average of CI values. The CI values at 5 days post inoculation were shown. The grey dashed lines from top to bottom represent 10-fold enhanced colonization and 10-fold reduced colonization, respectively. (**C**), Volcano plot of the distribution of altered proteins. Red dots represent up-regulated expression proteins, and green dots represent down-regulated expression proteins and grey dots represent no significant expression difference (threshold > 1.5, $p < 0.05$). (**D** and **E**), Effect of FlgM on the colonization of the Δ*flhB* or Δ*flaA* mutant. The CI values at 5 days post inoculation were shown. (**F**), Western blot (WB) assay for different secretion of FlgM in the *V. cholerae* flagellar mutants. sup: supernatant, p: pellets. (**G**), Correlation analysis of FlgM secretion and CI values in adult mice model (ImageJ and Pearson method). The colors of red, green dots represent a higher, lower of colonization than WT, respectively. Significance was determined by *t*-test; *P*-values: ns, not significant, *, < 0.05, **, < 0.01, ***, < 0.001.

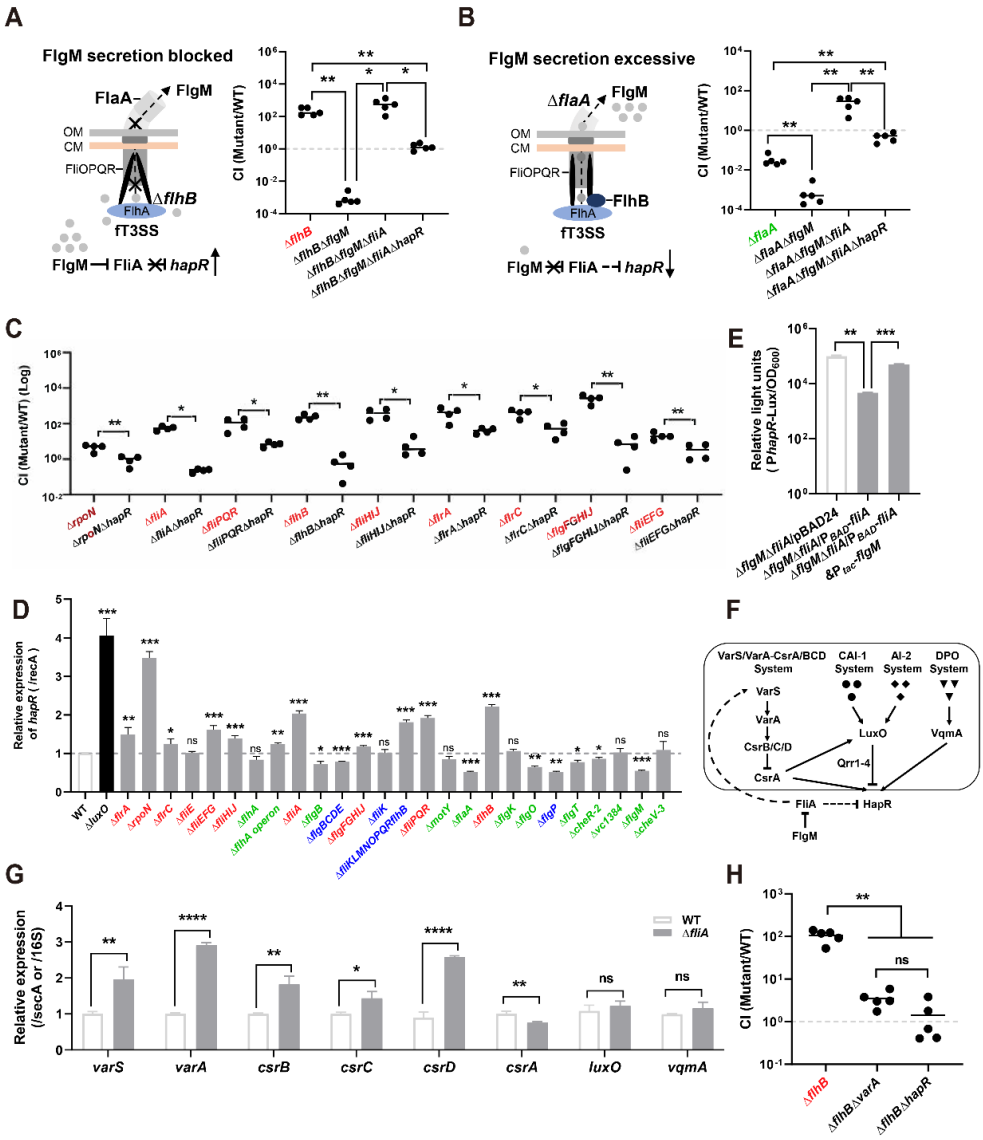

970

971 **Fig. 3. Intracellular FlgM deactivated FliA to promote *hapR* expression on**
972 **transcriptionally and post-translationally.** (**A** and **B**), Schematic diagram of FlgM
973 secretion in Δ*flhB* and Δ*flaA*, and the corresponding role of FlgM-FliA-*hapR* pathway
974 in colonization, respectively. (**C**), RT-PCR results of *hapR* expression in flagellar
975 mutants with enhanced colonization. The *recA* was used for normalization and Δ*luxO*
976 was used as a positive control. (**D**), *In vivo* competition experiments of different *hapR*
977 mutants in adult mice. The CI values at 5 days post inoculation were shown. (**E**), Effect
978 of FlgM and FliA overexpression on *hapR* expression. (**F**), Quorum sensing (QS)
979 regulatory network of *V. cholerae*. (**G**), Gene expression in the QS regulatory pathway.
980 Gene expression was normalized by *16S rRNA*, except for small RNAs called *csrBCD*
981 which were normalized by *secA*. (**H**), Role of the VarS/VarA-CsrA/BCD system in
982 adult mice colonization. The CI values at 5 days post inoculation were shown. The
983 colors of red, green, blue dots represent a higher, lower of colonization than WT or
984 same level, respectively. Significance was determined by *t*-test and one-way ANOVA
985 analysis; *P*-values: *, < 0.05, **, < 0.01, ***, < 0.001, ****, < 0.0001.

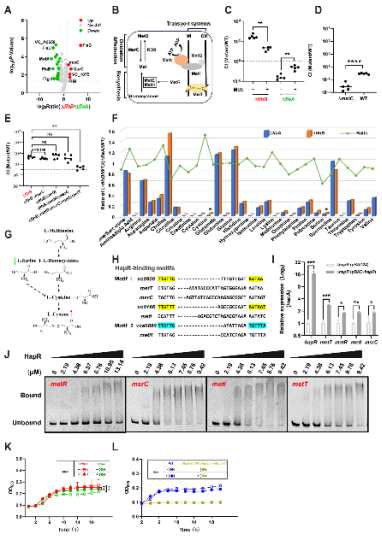

Fig. 4. HapR regulates *V. cholerae* colonization through methionine metabolism and transportation. (**A**), Volcano map of the precipitated proteomic of Δ*flhB*/Δ*flaA*. Red dots represent up-regulated expression proteins, and green dots represent down-regulated expression proteins and grey dots represent no significant expression difference (threshold > 1.5, $p < 0.05$). (**B**), Schematic diagram of methionine (Met) metabolism. (**C**), Effect of Met addition (in drinking water) *in vivo* on the colonization of Δ*flhB* and Δ*flaA*. (**D**), Effect of *msrC* in precipitated proteomic on the colonization of Δ*flhB* mutant. (**E**), Effect of indicated mutants on the colonization of Δ*flhB,* Δ*flhB*Δ*msrC*, Δ*flhB*Δ*metR*, Δ*flhB*Δ*metR*Δ*msrC*, Δ*flhB*Δ*metR*Δ*msrC*Δ*metI*Δ*metT*. (**F**), Amino acids and its derivatives were quantified by UPHLC. The column diagram represents the contents of amino acid and its derivatives in Δ*flhB* and Δ*flaA*. The line chart represents the ratio of amino acid and its derivative content of Δ*flhB*/Δ*flaA*. (**G**), Metabolic pathway of methionine converted to other amino acids. Methionine can be converted to homocysteine by demethylation, which subsequently forms cysteine together with serine. Two molecules of cysteine synthesize cystine, while serine itself can be converted to cysteine. The metabolic pathway was annotated by Kyoto Encyclopedia of Genes and Genomes. (**H**), Promoter sequence alignment of *metR*, *msrC*, *metI*, and *metT* with conserved two HapR binding Motifs. Yellow shading represents the conserved binding sequence of Motif 1 and aqua shading represents the conserved binding sequence of Motif 2. (**I**), Effect of *hapR* overexpression on the expression of *metR*, *msrC*, *metI*, and *metT*. The bars represent the corresponding standard deviations. (**J**), EMSA for HapR binding to the promoters of *metR*, *msrC*, *metI*, and *metT*. (**K**), Growth curve of Δ*flhB* and Δ*flaA* in the MM medium with or without 0.01mM L-Met. (**L**), Growth curve of WT, Δ*flhB*Δ*metR*Δ*msrC*Δ*metI*Δ*metT* in the MM medium with or without 0.01mM L-Met. The colors of red, green, blue dots represent a higher, lower of colonization than WT or same level, respectively. The CI values at 5 days post inoculation were shown. The horizontal bars indicate the averages of CI. Significance was determined by *t*-test and one-way ANOVA methods; *P*-values: ns, not significant, *, < 0.05, **, < 0.01, ***, < 0.001.

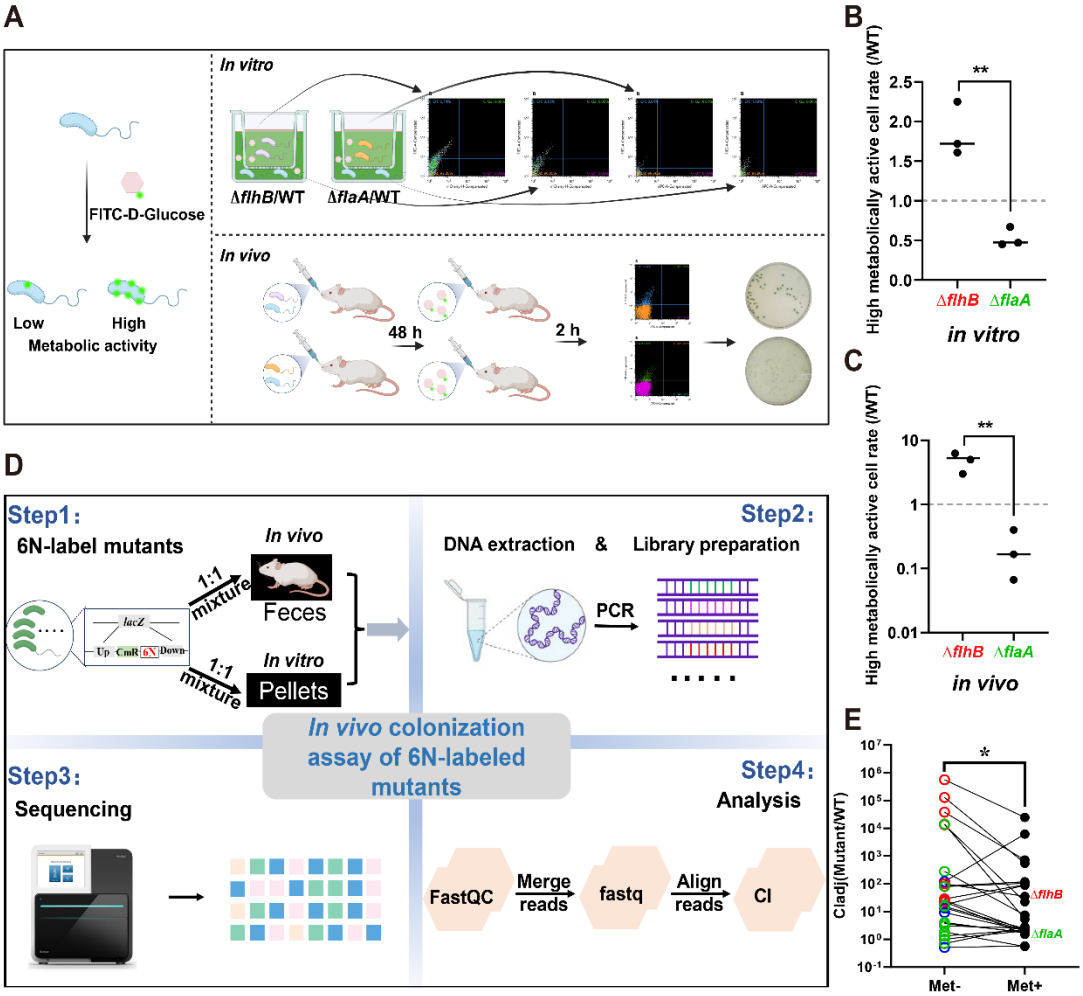

Fig. 5. Methionine-related metabolic activity affects *V. cholerae* colonization. (**A**), The workflow for metabolic activity assay with FITC-D-Glu-labeled method in vitro and in vivo. The figure was created by BioRender. (**B**), Flow cytometry analysis of wild-type co-with Δ*flhB* and wild-type co-with Δ*flaA* FITC-D-Glu-labeled in transwell chamber at 30 min. (**C**), The bacterial metabolic activity of wild-type co-with Δ*flhB* and wild-type co-with Δ*flaA* *in vivo* at 48h post-inoculation. (**D**), The workflow of colonization assay of 6N-labeled mutants *in vivo*. (**E**)**,** Colonization assay of 6N-labeled mutants *in vivo*. The raw data was analyzed by Vsearch and Python. The adjusted CIs of all flagellar mutants were analyzed by was calculated as the reads of mutant to WT colonies normalized with the input reads. The colors of red, green, blue dots represent a higher, lower of colonization than WT or same level, respectively. Significance was determined by *t*-test and one-way ANOVA methods; *P*-values: ns, not significant, *, < 0.05, **, < 0.01, ***, < 0.001.

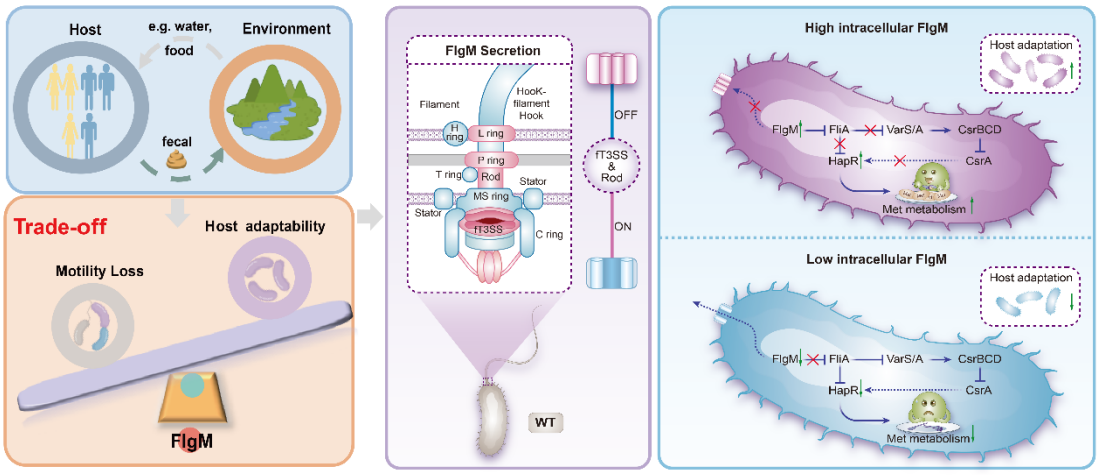

Fig. 6. Trade-off mechanisms between motility loss and host adaptability Mechanism. *Vibrio cholerae* predominantly cycles between aquatic reservoirs and the human host. Humans become infected by ingesting water or food contaminated with *V. cholerae*. The bacteria then colonize the small intestine, where they adapt by modulating their gene expression profile. Ultimately, they are shed back into the aquatic environment via feces, completing the transmission cycle and enabling potential new rounds of infection. A systematic analysis of cholera-associated samples collected from diverse environmental niches revealed a recurrent pattern of flagellar gene mutations in *V. cholerae* populations. Follow-up experimental investigations elucidated a fundamental trade-off mechanism, whereby the loss of bacterial motility is counterbalanced by enhanced adaptation to the host. In details, we analyzed 3,135 cholera-related samples and identified a recurrent pattern of flagellar mutations in *V. cholerae*, with notable clustering in genes including *flhB*, *fliA*, *fliF*, *fliD*, and *fliM*. A high-throughput screen of a comprehensive flagellar mutant library established a clear inverse correlation between a strain's capacity to colonize the host and its level of FlgM secretion. Specifically, elevated intracellular concentrations of FlgM inhibit the alternative sigma factor σ^{28} (FliA). This inhibition, in turn, relieves the repression on the transcription of *hapR*, which encodes the master regulator of quorum sensing. The subsequent upregulation of HapR activates genes involved in methionine metabolism and transport. This metabolic reprogramming ultimately enhances the colonization fitness of *V. cholerae* within the host. Employing a specially constructed, competitively matched pool of 6N-labeled mutant strains in an adult mouse model, we provided direct *in vivo* validation. These experiments confirmed that the loss of motility confers a selective advantage for environmental persistence, a phenotype mediated through the defined FlgM-FliA-HapR-methionine regulatory axis.